J Mater Sci (2010) 45:4631–4644
DOI 10.1007/s10853-010-4643-9

ULTRAFINE GRAINED MATERIALS

Microstructure evolution of CuZr polycrystals processed by high-pressure torsion

Milan Dopita · Miloš Janeček · Radomír Kužel · Hans Jürgen Seifert · Sergey Dobatkin

Received: 12 February 2010 / Accepted: 21 May 2010 / Published online: 10 June 2010

Abstract The microstructure evolution of extruded Cu–0.18 wt% Zr polycrystals processed by high-pressure torsion (HPT) at room temperature at the pressure of 4 GPa and the different number of the HPT revolutions (i.e. different strain) was investigated using the combination of the electron back-scatter diffraction, microhardness measurements and the X-ray diffraction. A significant transition from the inhomogeneous microstructure after few HPT revolutions into the homogeneous equiaxed microstructure with increasing number of HPT rotations was observed. HPT straining leads to the grain size refinement by a factor more than 100 after the 25 HPT revolutions. Moreover, the EBSD revealed an increase in the fraction of high-angle grain boundaries (HAGBs) with increasing HPT straining reaching the value of 70% after 25 revolutions. Additionally, a slight increase of the twin-related CSL Σ3 grain boundaries occurred during the microstructure refinement. The microhardness measurements confirmed the billet radial inhomogeneity at early stages of the HPT straining, whereas with increasing number of the HPT rotations, causing the specimen fragmentation and homogenization, the microhardness values increased. The average crystallite size and the average dislocation density in individual specimens determined by the XRD diffraction were in the range of approximately 100–200 nm and 2×10^{15} m^{-2}, respectively. Moreover, XRD measurements confirmed the absence of residual stresses in all specimens.

M. Dopita · H. J. Seifert
TU Bergakademie Freiberg, Institute of Materials Science, Freiberg, Germany

M. Janeček (✉)
Department of Physics of Materials, Faculty of Mathematics and Physics of the Charles University in Prague, Prague, Czech Republic
e-mail: janecek@met.mff.cuni.cz

M. Dopita · R. Kužel
Department of Condensed Matter Physics, Faculty of Mathematics and Physics of the Charles University in Prague, Prague, Czech Republic

S. Dobatkin
A. A. Baikov Institute of Metallurgy and Materials Science, Russian Academy of Sciences, Moscow, Russia

Introduction

The possibility of producing nanocrystalline (grain size smaller than 100 nm) and submicrocrystalline (grain size in the range 100–1000 nm) structures has been reliably established for various severe plastic deformation (SPD) techniques, such as equal-channel angular pressing (ECAP), multiaxial deformation, twist extrusion, accumulative roll bonding, etc. [1–4]. Grain refinement down to a nano- and submicro-level results in a significant increase in the strength at satisfactory ductility and leads to an increase of service properties, such as fatigue strength, cold resistance, superplasticity, wear resistance, etc. These enhanced physical properties have been found in a wide range of metallic materials and used in many industrial applications [1–4].

Particular attention is now being given to the studies of structure and properties of copper alloys after SPD for the purpose of their use in the electrotechnical industry. However, almost all reported results relate to ECAP of copper and its alloys [5–12]. ECAP gives the opportunity to produce rather large ingots, nevertheless under quite low pressures only. In this connection, it is interesting to study extreme structural states of commercial copper alloys and their mechanical behaviour. In order to create the extreme

state, high pressures and strains are required; they can be realized, e.g. during high-pressure torsion (HPT) on a Bridgman anvil [13, 14]. HPT allows: (i) to obtain effective grain refinement among numerous ways of SPD, (ii) to model phase and structural transformations at SPD (the decomposition of supersaturation solid solutions, the dissolution of particles of the second phase etc.), (iii) to study the heterogeneity of structure and properties at deformation development in connection with specific features of the scheme of deformation, and (iv) to recommend optimum regimes of ECAP and other modes of SPD, allowing receiving rather massive samples.

The objective of this investigation is to study the structure formation and the heterogeneity of microstructure of Cu–0.18 wt% Zr alloy prepared by the HPT process at different number of the HPT revolutions. The description of fragmentation of the microstructure introduced by the HPT and the correlation of microstructural properties as a grain/sub-grain sizes, grain boundary types and its character distributions and the deformation state of sample with its microhardness variations due to strain introduced to the material by this technique of severe plastic deformation are other issues in this experimental study.

Experimental procedures

Binary Cu–0.18 wt% Zr polycrystals were received in the as-cast condition. The material was hot extruded at the temperature of 500 °C using extrusion ratio of 12.25. The initial as-extruded material consists of relatively large grains (of the mean grain size of approximately 40–50 μm), which are internally deformed by the extrusion procedure.

The specimens for HPT were machined from the extruded bar. The HPT was performed in a 'groove' on samples of 10 mm in diameter and 0.6 mm in height at room temperature and the pressure of 4 GPa. The series of specimens after 1, 3, 5, 10, 15 and 25 revolutions was prepared for this investigation.

The microhardness profiles through the diameter of individual specimens were measured using the Micro-Vickers Hardness Tester Model 402 MVD (Wolpert Wilson, Wolpert Wilson Instruments, Aachen, Germany) at a load of 25 g.

The microstructure evolution and its fragmentation were investigated by electron back-scatter diffraction (EBSD). EBSD measurements were performed using the high-resolution scanning electron microscope LEO-1530 (Carl Zeiss, Carl Zeiss Semiconductor technologies A.G., Jena, Germany) equipped with a field emission cathode and Nordlys II EBSD detector (HKL Oxford Instruments, Oxford Instruments Nanoanalysis, Bucks, UK). The measurements were carried out at the acceleration voltage of 20 kV, working distance of 15 mm, the sample tilt of 70° and the high current mode was used for the Kikuchi pattern collection. The step size of measured maps was varied from 50 to 500 nm, depending on the grain size (i.e. the number of HPT revolutions and the position of the measured map in the sample). For identification and indexing of Kikuchi patterns and measured data evaluation the software package Channel 5 (HKL Oxford Instruments) was employed.

In order to get statistically relevant results, several EBSD orientation maps were accumulated in each sample differing in the number of the HPT revolutions (1–25 HPT revolutions). For all specimens some maps were measured in the centre of the sample. To get an overview of the changes of microstructural properties in dependence on the distance from the billet centre additional EBSD maps were measured at different distance from the sample centre and finally several maps were measured at the samples periphery as well. The EBSD investigations were performed on the plane perpendicular to the rotation axis of the HPT specimens.

Since the EBSD measurement is highly surface sensitive method and measured information comes from depth of several tenths of nanometers of the specimen it is necessary to prepare the sample surface properly. In particular, sample regions strained and disturbed by the specimen cutting have to be removed. The polishing procedure followed several steps. First, the specimens were mechanically ground using silicon carbide grinding plates with decreasing roughness and consequently polished with 6, 3 and 1 μm diamond paste. As a final polishing step the ion beam etching procedure was applied. The ion beam etching was performed using the Dual Ion Mill 600 (GATAN, GATAN Inc., Pleasanton, CA, USA). The specimen surface was etched with Ar ions accelerated to 5 kV. The angle between the incoming ion beam and the specimen surface was 20°, the sample was rotating during the etching and the total etching time was 120 min. In all samples under study, approximately one half of the sample thickness was removed during the polishing procedure to ensure the EBSD measurements to be performed from the middle of the sample thickness.

Due to the combination of its good spatial and angular resolution, the EBSD measurements provide the unique information on the specimen morphology, grain/sub-grain size distributions, the grain boundary misorientation and character distributions, as well as information about the deformation state of specimens and local preferred orientation of crystallites.

X-ray diffraction (XRD) measurements were performed with the aid of X'Pert Pro powder diffractometer (Panalytical B.V., PANalytical B.V., Almelo, The Netherlands),

filtered Cu$K_\alpha$radiation, variable divergence and anti scatter slits enhancing high-angle peaks important for line profile analysis and the PIXCel (PANalytical B.V., Almelo, The Netherlands) position sensitive detector that enables to obtain high-quality low-noise data at reasonable collection time. Line profile analysis was done by the simplified integral breadth method and the total pattern fitting [15, 16]. The method was used for the analysis of crystallite size, strain including dislocation-induced line broadening, possibly stacking faults and twins. Texture was evaluated simply from the conventional Bragg–Brentano symmetrical scans in terms of the Harris texture indices [17].

Results and discussion

Microhardness measurements

The deformation degree at HPT depends on the radius and the thickness of the sample: the thicker is the sample and the smaller is the radius, the smaller is the strain. At a constant thickness of the sample as in our case, the deformation degree increases with increasing distance from the centre that leads to changes of the structure and properties, i.e. to heterogeneity [14, 18]. In this connection a heterogeneity of microhardness values along two mutually perpendicular diameters of the sample on a surface in contact with an immobile deforming anvil (plane 1), on a plane passing through the middle of a thickness of the sample (plane 2) and on a surface in contact with a mobile (rotating) deforming anvil (plane 3) after 3, 5 and 15 HPT revolutions was studied. In Fig. 1 the average values of microhardness Hv measured along two mutually perpendicular diameters are presented.

It is seen that with increasing strain:

- the heterogeneity of microhardness values along the diameter of samples decreases;
- the difference of Hv values between the centre of the sample and edges decreases at the expense of an increase in Hv values in the centre;
- the area of the sample near edges where Hv reaches its maximum, increases.

The dependence of Hv on strain due to HPT was found to differ as a function of the distance from the specimen centre. At sample periphery Hv values do not change significantly with increasing strain, i.e. already after three HPT revolutions the 'steady' state is reached ($Hv_{sat} \approx$ 160–170 MPa). On the other hand, in the specimen centre a continuous increase of Hv with increasing strain up to 15 HPT rotations was observed.

Detailed inspection of Hv data does not reveal any statistically important difference between Hv values on both surfaces and in the centre throughout the whole sample diameter. All corresponding values lie within the experimental scatter indicated by error bars for each experimental point. Several exceptions are probably caused by experimental setup (slight misalignment of both anvils) and by different friction between the sample and mobile and immobile anvil.

Our measurements confirmed the well-known dichotomy of local microhardness results. First, the homogeneity variation across the specimen processed by HPT with lower hardness in the centre of the disc and higher values in the peripheral regions. These results were reported for azustenitic steel [19], Cu [20], high purity Ni [21], etc. Second, the continuous decrease of this heterogeneity with increasing torsional straining towards almost homogeneous Hv distribution when the specimen is strained to sufficiently high total strain as reported, e.g. in commercial purity Al [22], Cu [23] and Ni [18].

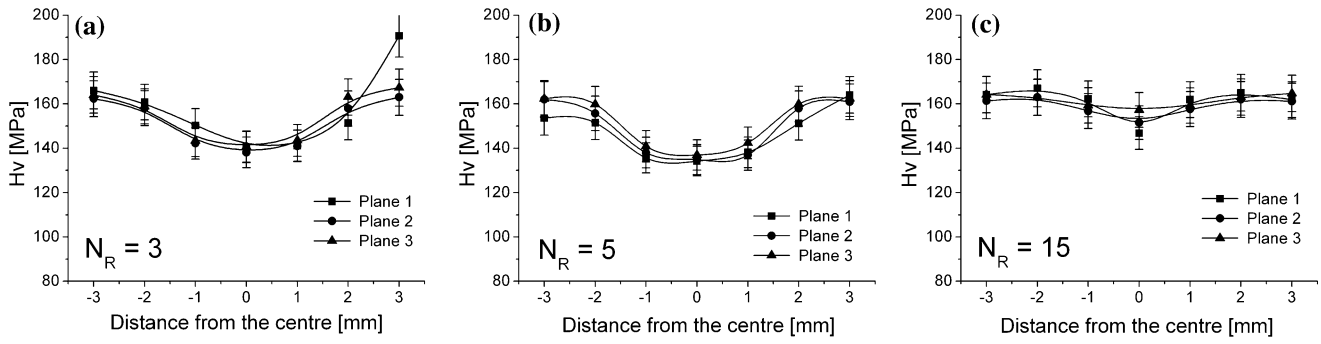

Fig. 1 Distribution of microhardness values as a function of the distance from the sample centre (microhardness profiles) in samples after 3, 5 and 15 HPT revolutions. Plane 1 - the surface in contact with the immobile deforming anvil. Plane 2 - the plane passing through the middle of the thickness of the sample. Plane 3 - the surface in contact with the mobile (rotating) deforming anvil

Microstructure evolution

Microstructure/morphology evolution

Due to the nature of the HPT material processing, where the induced strain (deformation) depends on the radial distance from the sample (billet) centre [24] it is obvious that HPT process produces radially inhomogeneous samples. With increasing number of revolutions the inhomogeneities in the microstructure of material tend to disappear and after a specific number of revolutions, depending on the initial material condition, the diameter and the thickness of the billet, and applied pressure, the microstructure of sample becomes homogeneous.

In studied samples, three regions differing in the specimen morphology were observed. Two volume dominant zones are: the *centre* of the sample (the central region marked as region 3 in Fig. 2a) consisting of relatively big internally deformed grains, and the *periphery* of the billet (the periphery region marked as region 1 in Fig. 2a) having refined small equiaxed grains. In between these two dominant zones an intermediate, rather subtile region (marked as 2 in Fig. 2a) was observed. This region exhibits spiral-like lamellar structure, whereas the lamellae contain more or less small equiaxed grains. The morphology of all three different zones observed in samples under study is shown as IPF coloured orientation map in Fig. 2c, d.

At a low number of HPT revolutions the inhomogeneous regions 3 and 2 prevail in the sample. With increasing number of the HPT rotations the volume fraction of the microstructurally homogeneous region 1 containing refined grains increases at the expense of the regions 2 and 3, and propagates towards the sample centre. After a certain number of HPT revolutions, in our samples more than 15, the inhomogeneous zones 2 and 3 disappear and the whole sample consists of homogeneous refined equiaxed grains of region 1. The evolution of the sample central region diameter, roughly estimated from the optical micrographs taken at etched samples, as a function of the number of HPT revolutions is shown in Fig. 2b.

In Fig. 3 the map of the centre of the disc after 15 HPT revolutions is shown. The rest of the central region (region 3) having the radius of about ~ 50 μm is clearly visible in the maps (region enclosed by a dashed circle in Fig. 3).

Exhaustive discussion of the definition of strain imposed during the HPT processing allowing calculation of different strain types (the true accumulated strain, shear strain, equivalent von Mises strain, the equivalent strain and the true strain) using different models can be found in [14]. We can calculate the von Mises strain $\varepsilon_{\text{von Mises}}$ using equation

$$\varepsilon_{\text{von Mises}} = \frac{\gamma}{\sqrt{3}}, \quad \gamma = \frac{2\pi r N_{\text{R}}}{h}, \tag{1}$$

where, γ denotes the shear strain, r is the radius of the specimen, N_{R} the number of whole HPT revolutions and h is the thickness of the specimen. Another important quantity describing the deformation imposed into the specimen during the HPT straining, taking directly into account the change of the specimen thickness during HPT processing, is the true strain $\varepsilon_{\text{true}}$ defined in [14] as

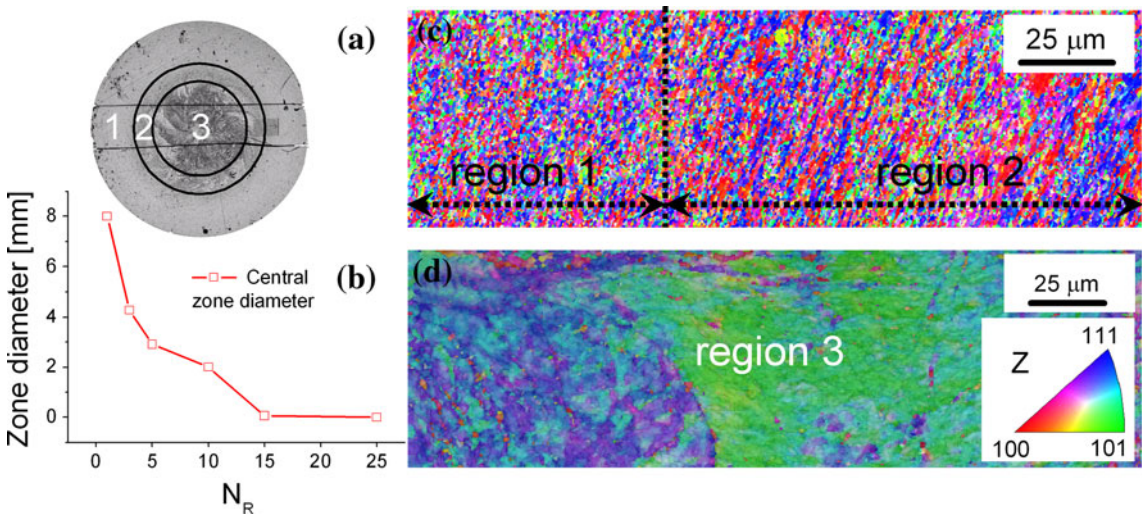

Fig. 2 Optical micrograph of the etched HPT processed sample after three HPT revolutions (**a**). Three morphologically different zones of the sample are marked in the micrograph. Note that the zone 2 (region enclosed between two *black circles*) is due to synoptic reasons enlarged in the sketch. The evolution of the sample central zone diameter, roughly estimated from the optical micrographs taken at etched samples, as a function of the number of HPT revolutions (**b**). IPF coloured orientation map of the region 1 and region 2 of the sample after three HPT revolutions (**c**). IPF coloured orientation map of the central part of billet (region 3) of the sample after three HPT revolutions (**d**)

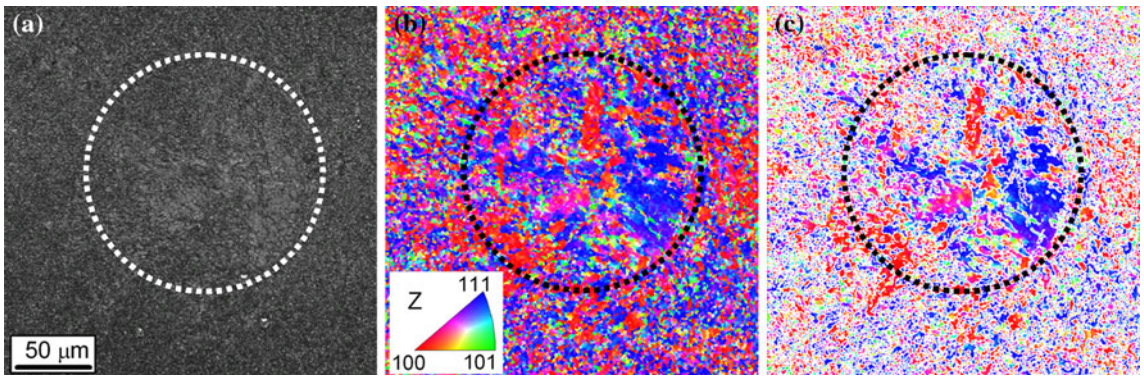

Fig. 3 The image quality map (**a**), the IPF coloured orientation map (**b**) the IPF coloured orientation map with highlighted HAGBs (misorientation >15°) plotted as *white lines* (**c**), measured in centre of the sample after 15 HPT revolutions. The dotted circle with radius ~50 μm encloses the rest of the central region (region 3) of the HPT specimen

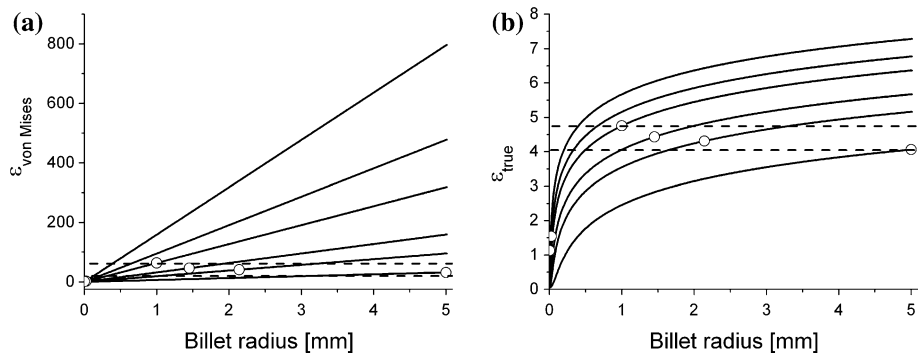

Fig. 4 Von Mises—$\varepsilon_{von\ Mises}$ (**a**) and the true strain—ε_{true} (**b**) calculated using Eqs. 1 and 2, respectively, as a function of the billet radius for 1, 3, 5, 10, 15 and 25 HPT revolutions (from bottom to the top). The *circles* correspond to the radius of the central region (region 3—i.e. the inner region having inhomogeneous deformed microstructure). The *dashed lines* enclose the strain interval, where the fragmented homogeneous microstructure starts

$$\varepsilon_{true} = \ln\left[1 + \left(\frac{2\pi r N_R}{h}\right)^2\right]^{\frac{1}{2}} + \ln\left(\frac{h_0}{h}\right), \qquad (2)$$

where h_0 is the initial thickness of the specimen and other variables have similar meaning as defined in Eq. 1.

In Fig. 4a, b von Mises and the true strain calculated using Eqs. 1 and 2, respectively, as a functions of the specimen radius for 1, 3, 5, 10, 15 and 25 HPT revolutions are shown ($h_0 = 0.6$ mm, $h = 0.57$ mm). The dependence of von Mises and true strain on the specimen radius as well as on the number of HPT revolutions is clearly visible in figures. The circles in Fig. 4a, b correspond to the radius of the central region (region 3—i.e. the inner region having inhomogeneous deformed microstructure). From these points we can roughly estimate the imposed von Mises and true strain at which the transition from inhomogeneous to fragmented homogeneous microstructure (transition from region 3 to region 1) occurs in the investigated samples. At low number of the HPT revolutions (between 1 and 10), the true strain at which fragmentation of the microstructure starts lies in a relatively narrow interval between the values of $\varepsilon_{true} = 4.06$ and 4.75, for 1 and 10 revolution, respectively. This interval is shown by dashed lines in Fig. 4a, b. Note that the fragmented homogeneous region was not found in sample after 1 HPT revolution, therefore the true strain, where the fragmentation starts, has to be higher than 4.06. The true strains of microstructure fragmentation for samples after 15 and 25 HPT revolutions are significantly below this interval. The deviation from 'expected' true strain necessary for microstructure fragmentation can be caused by inaccurate inner diameter measurement (in sample after 25 HPT revolutions the inner region was even not found and therefore is taken to be zero) or by the non-validity of Eqs. 1 and 2 for calculation of the strain as the radius goes to zero (i.e. when approaching the rotation axis).

The above discussed results concerning the radial inhomogeneity of the HPT samples prove unambiguously that the microstructure and material properties of the HPT samples significantly differ in the specimen centre and at

its periphery. Since the intermediate region (region 2) is rather thin compared to the zones 1 and 3 we suppose that it does not influence the material properties significantly (note that region 2 in Fig. 2a is enlarged due to synoptic reasons). Moreover, because of its small thickness zone 2 was not found in all measured samples. Hence, in all studied samples the detailed EBSD measurements were done in both main zones 1 and 3. In the next text separate results will be discussed and presented for both these regions, in particular 1 (sample periphery) and 3 (sample centre). Simultaneously, the evolution of all derived microstructural parameters during the HPT straining will be presented as a function of the number of HPT revolutions and not the strain. The same approach is proposed in both HPT review papers by Zhilyaev and Langdon and Valiev et al. [14, 24].

Grain/sub-grain size evolution

The grain/sub-grain size distributions were determined from the measured orientation maps using the line intercept method. As a boundary between the different grains or sub-grains the misorientation of 15° or 2°, respectively, were adopted. The grain/sub-grain size distributions followed the lognormal distribution in all measured maps. The mean grain size of the sample central region decreased monotonously from approximately 9 μm after the first HPT revolution to 480 nm after the 25 HPT revolutions. More pronounced grain size refinement occurred in the specimen periphery. After the first HPT revolution, the equiaxed homogeneous morphology of the material was not observed yet, and as the initial mean grain size the similar grain size (approximately 9 μm) as in the sample central region was determined. After three HPT revolutions the equiaxed homogeneous morphology of the material was present at the sample periphery and the mean grain size decreased to approximately 460 nm. With increasing number of HPT revolutions the mean grain size further reduced. However, the grain size refinement was only moderate in comparison to the mean grain size reduction between the first and the third HPT revolution, whereas finally after 25 HPT rotations the mean grain size of the equiaxed homogeneous grains was approximately 320 nm. The plots of the mean grain size as a function of the number of the HPT revolutions for sample central and sample periphery zones are shown in Fig. 5a.

The mean sub-grain size decreases from approximately 1.6 μm for both sample zones after the first HPT revolution and approaches the value of 390 and 280 nm for the sample central region and for the sample periphery zone, respectively. Similarly, as in the mean grain size evolution the mean sub-grain size decreased monotonously with increasing number of the HPT revolutions in the sample central region, whereas in the sample periphery the fastest mean sub-grain size reduction was observed between the first and the third HPT revolution. The plots of the mean sub-grain size versus number of the HPT revolutions for sample central and periphery zones are shown in Fig. 5b.

Regarding the grain size evolution, we can conclude that HPT processing resulted in grain size reduction by a factor more than 100 after 25 revolutions in comparison with the original extruded coarse grained material. In the samples centre zone the grain size was continuously refined with increasing number of HPT revolutions, contrary to the sample periphery, where significant grain size reduction and the formation of the equiaxed homogeneous grain structure was observed already after three HPT revolutions.

In EBSD investigation the change of the average grain size is usually analyzed. Recently, Hebesberger et al. [25] investigated the grain size evolution in Cu processed by HPT and found it to decrease with increasing strain ultimately reaching the steady-state. The authors concluded that the misorientations between neighbouring structural elements (grains) increased with strain and finally attaining almost random distribution by processes that are analogous to conventional dynamic recrystallization. In Armco steel processed by HPT the authors [26] investigated grain sizes in two positions (2 and 4 mm from the disc centre) and found the mean grain sizes of 270 and 130 nm, respectively.

In our work, the analysis of the change of both the grain and sub-grain size during HPT was carried out for the first

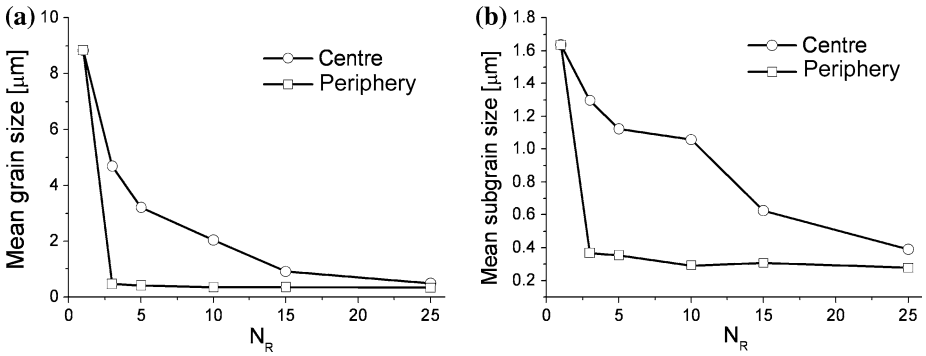

Fig. 5 The plots of the mean grain size as a function of the number of HPT revolutions for sample central (*open circles*) and sample periphery (*open boxes*) zones (**a**). Evolution of the mean sub-grain size versus number of HPT revolutions for sample central (*open circles*) and periphery (*open boxes*) zones (**b**)

time. It was shown that sub-grain refinement proceeds more slowly than grain refinement (cf. Fig. 5). It confirms the hypothesis that low-angle boundaries are more stable and are less mobile than high-angle boundaries [27]. The only similar comprehensive investigation of grain boundary evolution during ECAP was performed by Zhilyaev et al. on pure Ni [28]. The authors found similar differences in grain and sub-grain refinement across the specimen diameter. They report slightly smaller mean grain sizes of 270 and 210 nm in the central part and at the periphery.

Misorientation evolution and grain boundary characteristics

The determined crystal orientation of each point of measured EBSD map, as a basic output from the EBSD measurement, allows calculating the orientation relationship between pairs of distinct points—so called misorientation. Basically two kinds of misorientation information can be extracted from EBSD measurements—the correlated and uncorrelated misorientation distributions. The correlated misorientation distribution based on the calculation of the misorientations between nearest neighbour points yields information about the character and the fraction of grain boundaries, while for the calculation of the uncorrelated misorientation distribution, randomly chosen pairs of measured orientations are used, which holds the information about the texture and the morphology of specimen.

Correlated and uncorrelated misorientation distributions of the sample central region in samples after different number of the HPT revolutions are shown in Fig. 6. Significant decay of low angle misorientations in the correlated misorientation distribution with the increase of the HPT revolutions number is clearly visible in the figures. Moreover, the uncorrelated misorientation distributions approach to the theoretical random distribution [29] with increasing HPT straining. This is a consequence of the microstructure fragmentation and transition from the inhomogeneous to equiaxed homogeneous morphology of the material.

Similar trend in the misorientation distributions evolution, i.e. the decay of the low angle misorientation with increasing HPT straining was also observed in the sample periphery zone (see Fig. 7). Direct comparison of the sample central and periphery zone misorientation distributions (compare Figs. 6, 7) reveal, however, fine differences in the evolution of both sample regions. The decay of the low angle misorientations in the correlated misorientation distribution is the most pronounced between samples after the first and the third HPT revolution (note the change of the scale in Fig. 7 for 1 and 3 HPT rotations). Furthermore, the uncorrelated misorientation distribution approaches more closely to the theoretical random misorientation distribution even after the third HPT revolution. This is again the consequence of the grain refinement and homogenization.

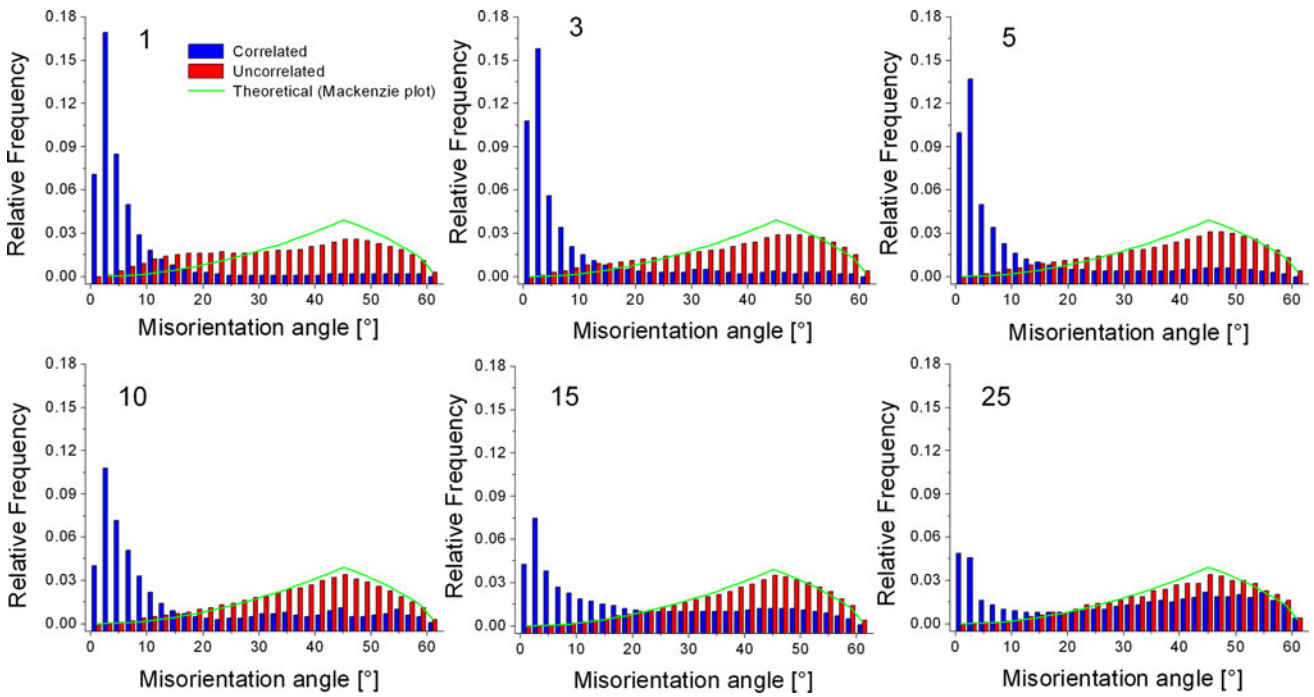

Fig. 6 Correlated and uncorrelated misorientation distributions for the sample central region in samples after 1, 3, 5, 10, 15 and 25 HPT revolutions. A *solid line* corresponding to the theoretical random distribution (so called Mackenzie plot) is shown in figures

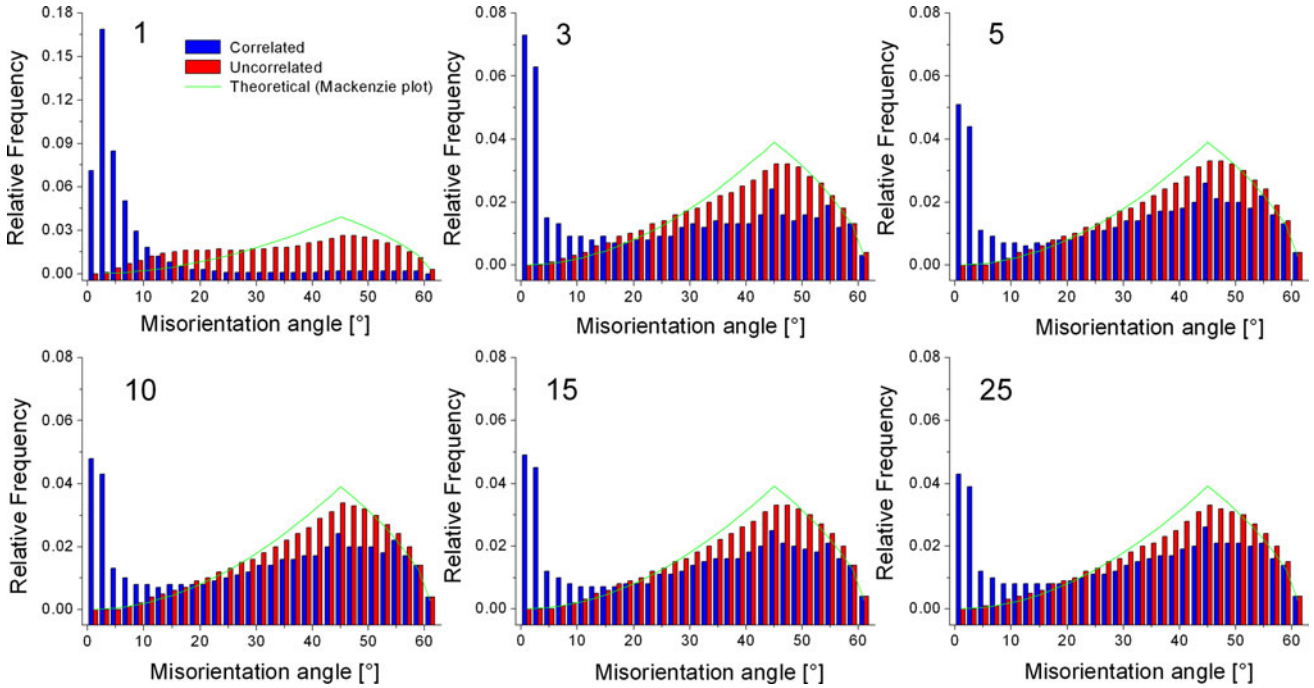

Fig. 7 Correlated and uncorrelated misorientation distributions for the sample periphery region in samples after 1, 3, 5, 10, 15 and 25 HPT revolutions. A *solid line* corresponding to the theoretical random distribution (so called Mackenzie plot) is shown in figures

The fraction of the low-angle grain boundaries (LAGBs) and HAGBs can be determined from correlated misorientation distribution. The LAGBs fraction can be calculated by integration of the correlated misorientation distribution to a certain limit. As a boundary between the LAGBs and HAGBs the angle of 15° derived by Brandon [30] was chosen.

In Fig. 8a, b the evolution of the LAGBs/HAGBs fractions as a function of the number of HPT revolutions for central and periphery zones of the specimens are shown. A pronounced evolution from initially prevailing fraction of the LAGBs to the higher amount of HAGBs with increasing number of HPT revolutions is clearly seen. After the first HPT revolution more than 90% of LAGBs were found in both central and periphery sample regions.

With increasing HPT straining (increasing HPT revolution number) the fraction of LAGBs linearly decreases and after 25 HPT revolutions the majority of GBs (about 70%) are HAGBs in the central sample zone. The decay of the LAGBs fraction versus the number of the HPT revolutions in the central zone of the specimen can be approximated by the linear function of the rotation numbers N_R: $\text{LAGBs}_{\text{fraction}}$ [%] = (92.79 ± 1.76) − (2.44 ± 0.14) × N_R. The decay of the LAGBs on the expense of the HAGBs after first three HPT revolutions is more rapid in the sample periphery (compare Fig. 8a and b). Finally, after five HPT revolutions the LAGBs/HAGBs ratio is saturated at value of about 30/70% in the specimen periphery and remains almost unchanged with additional HPT straining. The evolution of the grain boundaries with increasing HPT straining clearly demonstrates the transition from the nonequilibrium microstructure formed by large deformed grains filled with sub-grains enclosed by nonequilibrium grain boundaries towards an equiaxed homogeneous microstructure bounded by the equilibrium grain boundaries. The fragmentation, i.e. the transition from the nonequilibrium to equilibrium microstructure is completed already after five HPT revolutions and does not change significantly with additional HPT straining in the sample periphery. On the other hand, in the sample central region this process is continuous and follows the linear dependence with the number of the HPT revolutions.

As mentioned in the previous section, the only reported detailed investigation of misorientation distributions in specimens after HPT is the work of Zhilyaev et al. [28, 31] at pure Ni. The authors report high fraction of HAGBs of 66% and 67% both at the central part and at the periphery of the specimen after five HPT revolutions at 6 GPa. This corresponds well to the development of the fraction of HABGs at periphery of CuZr specimen, where the saturation value of 70% was found also after five HPT rotations. On the other hand, in the centre of the CuZr specimen, the evolution of HAGBs with strain is much slower reaching the majority only in the specimen after 20 rotations.

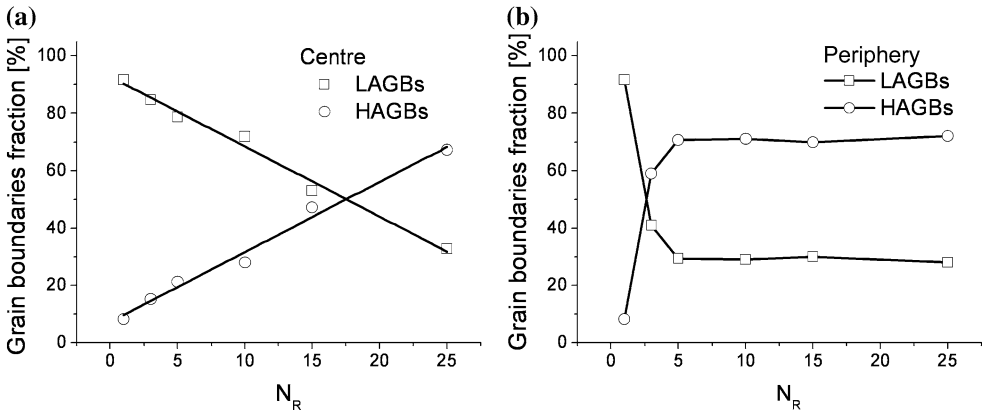

Fig. 8 Evolution of the fractions of low (LAGBs) and high (HAGBs) angle grain boundaries as a function of the number of HPT revolutions for the sample central region (*solid lines* correspond to the linear fit) (**a**) and sample periphery (**b**)

Details of the HAGBs, special CSL grain boundaries

The evolution of the HAGBs during the HPT straining can be described using the grain boundary distribution by the reciprocal density of coincidence sites Σ (CSL) theory. Brandon criterion $\Delta\theta = \theta_0\Sigma^{-1/2}$ [30], where $\Delta\theta$ is deviation from exact CSL angle, θ_0 is the LAGBs/HAGBs limit, and Σ is corresponding CSL, was adopted as a tolerance limit from exact CSL values.

In the sample central zone a continuous increase of the twin-related CSL Σ3 grain boundaries with increasing HPT straining was observed. The length frequency increased from approximately 0.3% after the first HPT revolution to about 2.5% after 25 HPT rotations. Simultaneously an increase of all CSL Σ <30 from about 1.2% to approximately 7.4% was observed. The aggregate sum of all CSL Σ <30 and Σ3 grain boundaries in the sample central zone as a function of the HPT revolution number is shown in Fig. 9a. In the sample periphery, the increase of all CSL Σ <30 and Σ3 grain boundaries is steep only to the third HPT revolution, contrary to the continuous increase of the CSL grain boundaries in the sample central zone. After three HPT revolutions the length frequencies of all CSL Σ <30 and Σ3 grain boundaries saturates at values of 7.5% and 2.3%, respectively, and remain almost unchanged with additional HPT straining (see Fig. 9b). The frequencies of the CSL grain boundaries of both sample central and periphery zones approach to similar values after the 25 HPT revolutions (compare Fig.9a and b). This is a consequence of the sample microstructure homogenization and fragmentation occurring during the HPT straining.

Grain boundary character distribution was also examined in pure Ni [28, 31]. Twin (Σ3) and other low Σ (Σ <30) special boundaries were also observed. Their fractions are slightly higher than in CuZr. Similarly as for HAGBs the difference is more pronounced in the central part of the specimen, while at the periphery almost the same fraction of twins was observed in Ni and CuZr.

The deformation state of the material

The results of EBSD measurements may be also used to classify the deformation state of the material. The classification is based on the character of misorientations determined by individual EBSD measurements within individual grains and allows characterizing the internal 'substructure' of individual grains. The volume fraction of differently 'substructured' grains may then define the deformation state of the specimen. Note, that the deformation state according to this definition is based on the misorientation and the range of its values only and as such

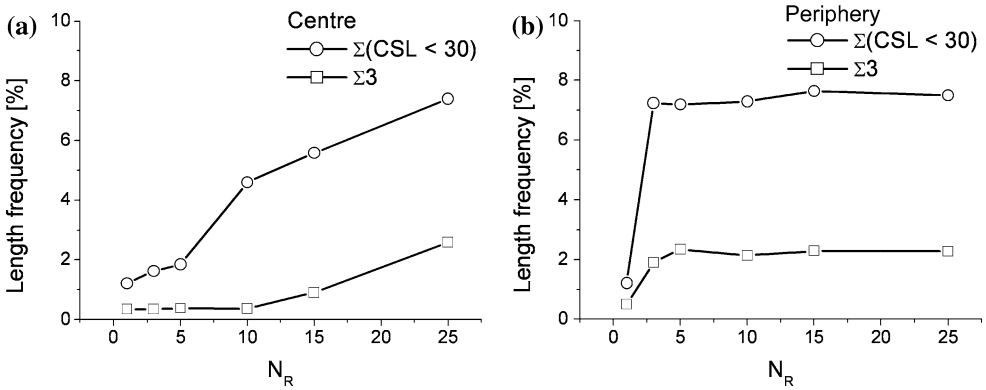

Fig. 9 Evolution of the twin-related Σ3 coincidence sites lattice (*open boxes*) and aggregate sum of all coincidence sites lattice (CSL Σ <30) smaller than 30 (*open circles*) as a function of the number of HPT revolutions for the sample central (**a**) and sample periphery (**b**) zones

it is not related to the deformation state of the grain in the general sense caused by torsional straining.

Based on the orientation mapping, we reconstruct first the individual grains, then estimate the average misorientation in each grain and finally calculate the deviations from this average misorientation within a grain. If the average misorientation angle in a grain exceeds the user-defined minimum angle to define a sub-grain, θc, the grain is classified as being 'deformed'. In this case the individual measured volumes of one grain have different orientations, which indicate that the grain is internally deformed. Some grains consist of sub-grains whose internal misorientation is below θc but the misorientation from sub-grain to sub-grain is above θc. In that case the grain is classified as 'substructured'. All remaining grains containing volumes of low misorientations only are classified as 'non-deformed'.

In Fig. 10a, b the deformation state of specimen as a function of HPT revolution number is shown. In both sample zones the specimen is deformed already before HPT processing. This deformation state of specimen is a consequence of the extrusion process which was applied to the coarse grained material before the HPT straining.

In the sample central zone the deformed volume fraction of the specimen decreases, while the non-deformed volume fraction increases with increasing number of the HPT revolutions. Both the deformed and nondeformed volume fractions follow the linear dependence and can be approximated by functions: Deformed [vol%] = $(90.5 \pm 2.6) - (3.15 \pm 0.22) \times N_R$ and Nondeformed [vol%] = $(4.4 \pm 1.2) + (2.83 \pm 0.10) \times N_R$. In the initial extruded material, more than 90% of the material is deformed while after the 25 HPT revolutions the ratio between deformed and nondeformed volume fraction of the sample is about 11/77% in the specimen central zone. In the sample periphery a steep increase of the nondeformed fraction at the expense of the deformed fraction between one and three HPT revolutions occurred. After the five HPT revolutions

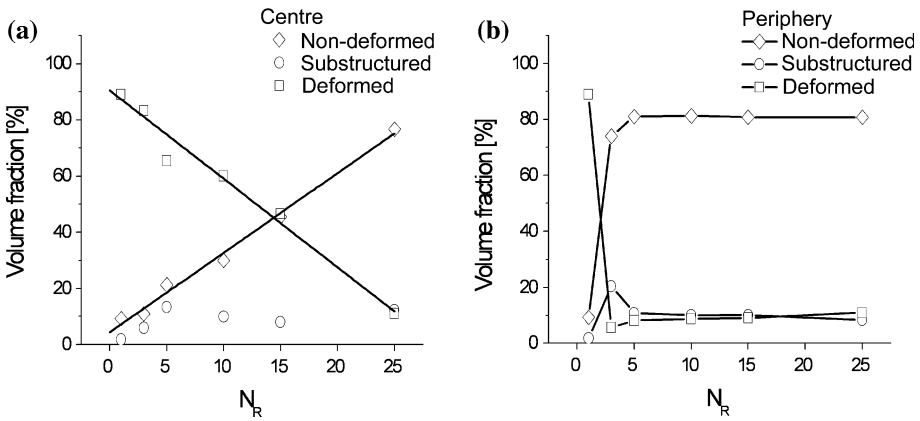

Fig. 10 Evolution of the deformation state of specimen determined from the EBSD measurements for sample central (**a**) and sample periphery (**b**) zones versus the number of the HPT revolutions. The volume fraction of recrystallized sample is represented by open diamonds, substructured fraction by the *open circles* and deformed fraction by the *open boxes*

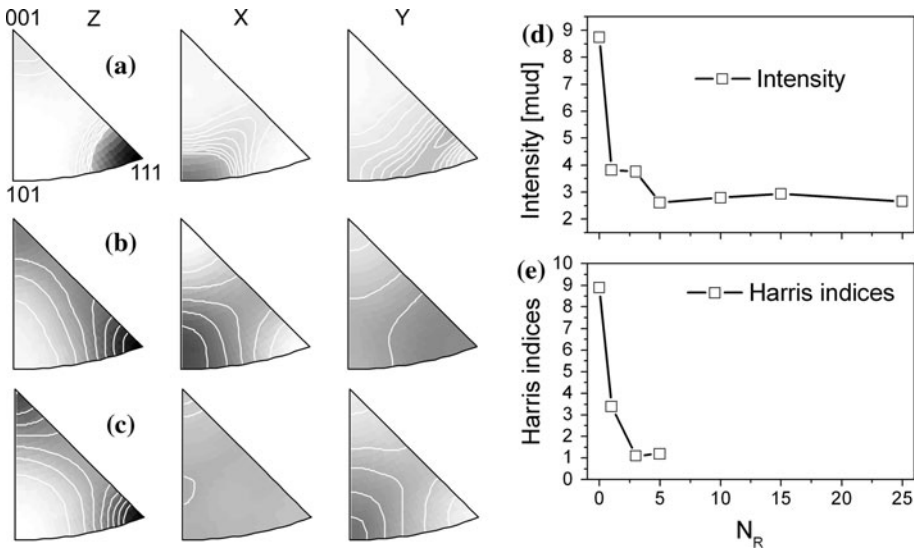

Fig. 11 Measured inverse pole figures corresponding to the orientation density in the z, x and y directions of the sample for the initial extruded material (**a**) and specimens after 5 (**b**) and 25 (**c**) HPT revolutions. The evolution of the maximum in the inverse pole figures at (111) pole as a function of the number of HPT rotations (**d**). The (111) Harris texture indices for the initial extruded material and specimens after 1, 3 and 5 HPT revolutions (**e**)

the ratio between the deformed and nodeformed fraction of sample is approximately 9/81% and does not change with additional HPT straining.

Microtexture evolution

In Fig. 11 measured inverse pole figures corresponding to the orientation density in the *z*, *x* and *y* sample directions of the initial material (Fig. 11a) and specimens after 5 (Fig. 11b) and 25 (Fig. 11c) HPT revolutions are shown. The initial extruded material exhibits strong (111) preferred orientation of crystallites. With increasing HPT straining the strength of the (111) texture component significantly decreases. The maximum in the inverse pole figure at (111) pole was nearly 9 mud (multiples of uniform distribution) in the initial material (Fig. 11a) and decreased with increasing HTP revolution number. Finally, the strength of the (111) component was approximately 2.5 mud in sample after 25 HPT revolutions, which corresponds to a weak texture. The evolution of the maximum in the inverse pole figure at (111) pole as a function of the number of HPT rotations is shown in Fig. 11d. The weakening of the (111) texture is a direct consequence of grain rotations occurring during the fragmentation and homogenization of the sample microstructure.

The microtexture evolution determined from the EBSD mapping corresponds well to the texture evolution determined from the XRD measurements. The Harris texture indices determined for initial extruded material were: hhh = 8.9, h00 = 0.6 and hh0 = 0.01, which demonstrates a strong (111) preferred orientation of crystallites in the initial sample. With HPT straining the strength of the (111) texture component decreases as it can be directly seen from the decay of the hhh Harris texture indices (see Fig. 11e).

XRD characterization

The detailed results of the X-ray characterization will be published elsewhere. The main results only are summarized here. Usually, the fixed irradiated area of 5 × 5 mm was used.

The lattice parameters of all investigated samples agree well with the tabulated values. This indicates the absence of significant residual stresses. They do not differ for various samples to quite high precision (0.3615 nm). The analysis of the integral breadths of XRD line profiles in terms of the modified Williamson–Hall (WH) plot shows that values of crystallite size are on the limit of detection by XRD profile analysis (100–200 nm). One example of the plot is shown in Fig. 12. In the first approximation, the intercept is inversely proportional to the crystallite size; the slope to the square-root of dislocation density and the line

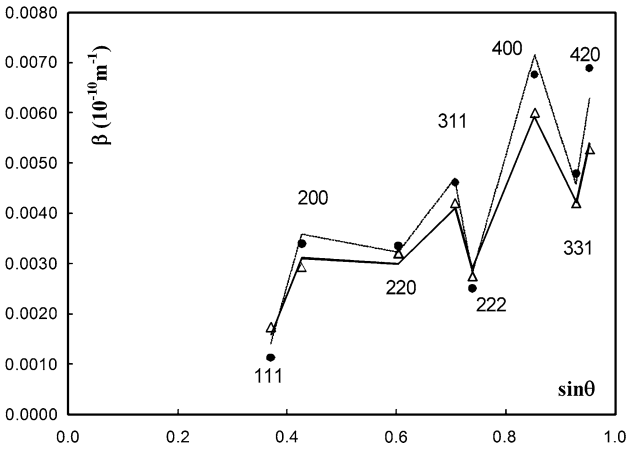

Fig. 12 Williamson–Hall plot (integral breadth $\beta(1/d)$ vs. sin θ) with indicated *hkl* indices. *Closed circle* 4 GPa, *open triangle* 2 GPa, correspond to experimental data after instrumental correction, lines connect corresponding calculated values

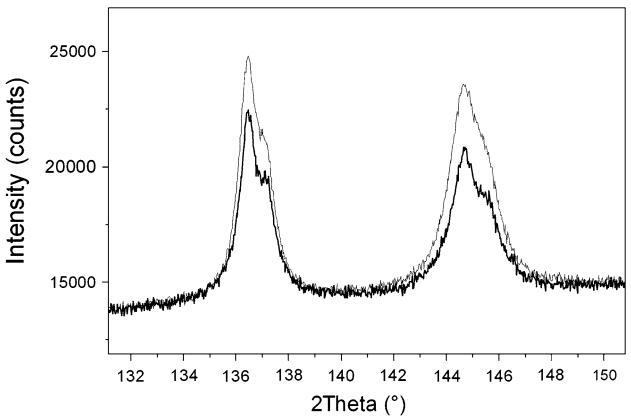

Fig. 13 A part of the diffraction pattern for sample after one HPT rotation. Diffraction peaks 331 and 420 taken in the specimen center (*thin line*) and specimen periphery 4 mm from the center (*thick bottom line*)

broadening anisotropy is given by elastic anisotropy and dislocation types. The plots do not differ significantly for different number of HPT revolutions and give dislocation densities of about 2×10^{15} m^{-2}.

In deformed copper, the WH plots generally exhibit line broadening anisotropy of the $\beta_{hhh} \ll \beta_{h00}$ type which can be well explained by dislocations with the Burgers vector $b \parallel \langle 110 \rangle$ that are typical for the face centred cubic (f.c.c.) structures (cf. Fig. 13). The magnitude of the anisotropy indicates prevailing screw dislocations. The only small change observed was an increase of profile tails after three revolutions with respect to the sample deformed by only one HPT revolution. Long profile tails can be caused by higher correlation in dislocation arrangement and/or by sample inhomogeneity.

Table 1 Structure parameters for samples deformed by different number of HPT rotations

Number of rotations	Position	ρ (10^{15} m^{-2})	FWHM/β	Texture index		
				111	100	110
1	Centre	1.3	0.75	3.4	0.8	0.2
1	2 mm from the centre	1.1	0.74	1.3	2.3	0.2
1	4 mm from the centre	1.7	0.71	1.4	1.5	0.4
3	Centre	1.7	0.68	1.1	1.1	0.6
3	3 mm from the centre	1.7	0.68	1.8	0.8	0.5
5	Centre	2.0	0.68	1.2	1.1	0.7
5	3 mm from the centre	2.0	0.68	1.9	0.8	0.5

ρ Dislocation density obtained by the simplified method, *FWHM/β* ratio of full-width-at-half-of-maximum and integral breath (smaller value means longer profile tails, 0.635 for Cauchy profile). Harris texture indices of *hkl* peak should be equal to unity for random grain orientation

Since systematic in-plane inhomogeneity of microstructure was observed by EBSD more local studies were also performed for a few selected samples. The results are shown in Table 1. Smaller regions of 1 × 2 (height) mm were irradiated in several positions on the specimen (centre, 2, 3, 4 mm from the centre). Differences, i.e. inhomogeneities could be observed, as expected, mainly on the samples after one and also after three HPT revolutions. For higher number of rotations no differences could be observed by XRD. While no significant differences are found in the absolute values of integral breadth, there are systematic changes in the profile shape. Profile tails are longer passing from the centre to the periphery of the specimen. As a consequence, a variation of the determined dislocation densities—a small increase from the centre to the periphery can be observed.

The differences in microstructure evolution of Cu and CuZr processed by HPT

The differences between Cu and CuZr in microhardness and the microstructure evolution will be discussed in terms of the influence of Zr additions. Our previous investigations [10–12] revealed the presence of very fine precipitates of Cu_9Zr_2 phase, which were homogeneously distributed within grains. These precipitates enhance significantly the thermal stability of ultrafine-grained CuZr processed by ECAP as has been reported by Molodova et al. [32]. However, due to their low volume fraction reported also in [32] their influence on overall microstructure evolution during HPT straining is probably rather marginal. On the other hand, due to a limited solubility of Zr in Cu [33] the influence of solutes can be also expected.

The saturation values of microhardness in Cu processed by HPT depend on the purity and range from 140 to 160 MPa [20, 34]. Our measurements of microhardness at the periphery of CuZr specimens yield the Hv ≈ 160–170 MPa. The slightly higher microhardness values in the alloy are consistent with the combined effect of solution and precipitation strengthening. The radial inhomogeneity of microhardness manifested by lower values of Hv in the central part than at the periphery both in Cu and in CuZr alloy is typical for all low and medium stacking fault materials and contradicts to the behaviour of pure Al where the opposite homogeneity with maximum in the central part was observed [33] and explained by much higher rate of dynamic recovery in high stacking fault energy materials.

The minimum grain/sub-grain size in Cu was measured by many authors usually by TEM [25, 34–36]. The observations gave grain sizes of ≈140 nm in the outer region and ≈350–300 nm in the central part. Our EBSD measurements in CuZr yielded slightly higher values of 390 nm at the centre and significantly higher values (280 nm) at the specimen periphery. This contradicts to the observations of the reduction of d_{min} in materials with lower stacking fault energy [37, 38]. The apparent disagreement may be explained by several ways. Recently, Hebesberger et al. [25] introduced the concept of structural elements rather than grain/sub-grains to characterize the microstructure in SPD materials. In Cu processed by HPT he found this structural element size to be ≈400 nm which is slightly bigger than our values determined by EBSD in CuZr. Another explanation may be simply the experimental technique used for minimum grain size determination. The values of grain size determined by X-rays are known to be smaller than by TEM [39]. Our X-ray measurements gave the average grain sizes in the range of 100–200 nm. Some small effect of precipitates on grain fragmentation in CuZr cannot be also excluded.

In CuZr enhanced twinning was observed reaching the saturation value of ≈2.5%. On the other hand, in HPT-processed Cu the twin density is very low (below 0.1%) [38]. Thus, the deformation mechanisms in CuZr include

both twinning and dislocation slip while in Cu only the latter mechanism is operating. This is consistent with lower stacking fault energy and slower rates of recovery in CuZr [37, 38]. Moreover, X-ray line profile analysis revealed high dislocation density $\rho = 2 \times 10^{15}$ m^{-2} in our specimens. Much lower dislocation density of approximately $\rho = 0.2 \times 10^{15}$ m^{-2} was found in pure Cu [38]. This apparent difference may be again explained by lower SFE in the alloy than in pure Cu. Reduction of SFE promotes splitting of dislocations and hinders their recovery by cross-slip or climbing.

Conclusions

The microstructure evolution of extruded Cu–0.18 wt% Zr polycrystals processed by high pressure torsion at room temperature, the pressure of 4 GPa and different numbers of the HPT revolutions (i.e. different strain) were studied by the combination of the electron back-scatter diffraction, microhardness measurements and the X-ray diffraction. The following conclusions may be drawn from this investigation.

The HPT straining produces radially inhomogeneous samples. With increasing number of HPT revolutions the inhomogeneities in the microstructure of material tend to disappear and after more than 15 HPT revolutions, the microstructure of sample becomes homogeneous.

Three distinct regions differing in the specimen morphology exist in studied samples during the HPT processing. Two volume dominant zones are: the centre of the sample consisting of relatively large internally deformed grains, and the periphery having refined small equiaxed grains. Between these two dominant zones an intermediate region, having spiral-like lamellar structure and containing small equiaxed grains, was observed. At a low number of HPT revolutions the inhomogeneous regions prevail in the sample. With increasing HPT straining the volume fraction of the microstructurally homogeneous region containing refined grains (periphery zone) increases at the expense of the inhomogeneous regions (centre of the sample), and propagates towards the billet centre.

The HPT straining results in significant grain refinement by a factor more than 100. The mean grain size of initial extruded material decreased from approximately 40–50 μm to the mean grain size of about 280 nm for the equiaxed homogeneous grains/sub-grains after 25 HPT revolutions.

A pronounced evolution from prevailing fraction of the LAGBs to the higher amount of HAGBs with increasing number of HPT revolutions was observed. After the first HPT revolution more than 90% of LAGBs were found in both central and periphery sample regions, while after the total fragmentation of the specimen microstructure the LAGBs/HAGBs ratio saturated at the value of about 30/70%.

A slight increase of the twin-related CSL Σ3 grain boundaries from approximately 0.3% after the first HPT revolution to about 2.5 length % in fragmented homogenized sample after 25 HPT rotations was observed in investigated samples.

Both, the EBSD and the XRD confirmed a pronounced decay of the strong (111) preferred orientation of crystallites, occurring in the initial extruded material, which was a consequence of the microstructure homogenization occurring during the HPT straining.

The microhardness measurements confirmed the specimen radial inhomogeneity at early stages of the HPT straining, whereas with increasing number of the HPT rotations, causing the specimen fragmentation and homogenization, the microhardness values increased.

The inhomogeneity of the specimens after few HPT revolutions was confirmed by the local XRD studies. Moreover, the XRD investigations yielded an average crystallite size of investigated materials in range of approximately 100–200 nm, confirmed the absence of the residual stresses and gave average dislocation densities of about 2×10^{15} m^{-2} in samples under study.

Acknowledgements The authors acknowledge funding of the Ministry of Education of the Czech Republic through the research program MSM 0021620834 and by the grants IAA101120803 and KAN400720701 of the Academy of Sciences of the Czech Republic. One of the authors M.D. acknowledges the financial support of this work through the Dr. Erich-Krüger-Stifftung.

References

1. Lowe TC, Valiev RZ (eds) (2000) Investigations and applications of severe plastic deformation. Kluwer Academic Publishing, Dordrecht, The Netherlands, p 395
2. Zehetbauer MJ, Valiev RZ (eds) (2003) Nanomaterials by severe plastic deformation. Wiley-VCH, Vienna, Austria, p 850
3. Horita Z (ed) (2005) Nanomaterials by severe plastic deformation. Trans Tech Publications Ltd., Switzerland, p 1030
4. Estrin Y, Maier HJ (eds) (2008) Nanomaterials by severe plastic deformation. Trans Tech Publications Ltd, Switzerland, p 1094
5. Neishi K, Horita Z, Langdon TG (2001) Scripta Mater 45:965
6. Patlan V, Suzuki Y, Kitagawa K, Kopylov VI, Vinogradov A (2002) Acta Mater 50:1639
7. Vinogradov A, Ishida T, Kitagawa K, Kopylov VI (2005) Acta Mater 53:2181
8. He W, Wang E, Hu L, Yu Y, Sun H (2008) J Mater Process Technol 208:205
9. Kužel R, Cherkaska V, Matěj Z, Janeček M, Čížek J, Dopita M (2008) Z Kristallogr Suppl 27:73
10. Dopita M, Janeček M, Rafaja D, Uhlíř J, Matěj Z, Kužel R (2009) Int J Mater Res 100(6):785
11. Janeček M, Čížek J, Dopita M, Král R, Srba O (2008) Mater Sci Forum 584–586:440
12. Kužel R, Janeček M, Matěj Z, Čížek J, Dopita M, Srba O (2009) Metall Mater Trans 41A:1174

13. Bridgman PW (1943) J Appl Phys 14:273
14. Zhilyaev AP, Langdon TG (2008) Prog Mater Sci 53:893
15. Matěj Z, Kužel R (2009) MStruct - program/library for Micro-Structure analysis by powder diffraction, available from http://xray.cz/mstruct/
16. Kužel R, Matěj Z, Nichtová L (2010) Powder Diffr (to be published)
17. Harris GB (1952) Philos Mag 43:113
18. Zhilyaev AP, Nurislamova GV, Kim BK, Baro MD, Szpunar JA, Langdon TG (2003) Acta Mater 51:753
19. Vorhauer A, Pippan R (2004) Scripta Mater 51:921
20. Jiang H, Zhu YT, Butt DP, Alexandrov IV, Lowe TC (2000) Mater Sci Eng A 290:128
21. Yang Z, Welzel U (2005) Mater Lett 59:3406
22. Zhilyaev AP, McNelley TR, Langdon TG (2007) J Mater Sci 42:1517. doi:10.1007/s10853-006-0628-0
23. Horita Z, Langdon TG (2005) Mater Sci Eng A 410–411:422
24. Valiev RZ, Islamgaliev RK, Alexandrov IV (2000) Prog Mater Sci 45:103
25. Hebesberger T, Stüwe HP, Vorhauer A, Wetcher F, Pippan R (2005) Acta Mater 53:393
26. Ivanisenko Y, Valiev RZ, Fecht H-J (2005) Mater Sci Eng A 390:159
27. Humphreys FJ (1996) Hetherly: recrystallization and related annealing phenomena. Pergamon, London, p 496
28. Zhilyaev AP, Kim B-K, Szpunar JA, Baro MD, Langdon TG (2005) Mater Sci Eng A 391:377
29. Mackenzie JK (1964) Acta Metall 12:223
30. Brandon DG (1966) Acta Metall 14:1479
31. Zhilyaev AP, Baro MD, Horita Z, Szpunar JA, Langdon TG (2004) Russ Metall 1:60
32. Molodova X, Khorashadizadeh A, Gottstein G, Winning M, Hellmig RJ (2007) Int J Mater Res 98:1
33. Wang N, Ch Li, Du Z, Wang F, Zhang W (2006) Comput Coupling Phase Diagr Thermochem 30:461
34. Horita Z, Langdon TG (2005) Mater Sci Eng A 410–411:422
35. Xu C, Horita Z, Langdon TG (2007) Acta Mater 55:203
36. Liao XZ, Zhao YH, Zhu YT, Valiev RZ (2004) J Appl Phys 96:636
37. Balogh L, Ungar T, Zhao Y, Zhu YT, Horita Z, Xu C, Lagdon TG (2008) Acta Mater 56:809
38. Zhao YH, Horita Z, Langdon TG, Zhu YT (2008) Mater Sci Eng A 474:342
39. Ungar T, Tichy G, Gubiza J, Hellmig RJ (2005) Powder Diffr 20:366